Chinese Chemical Letters 33 (2022) 4761–4765

Contents lists available at ScienceDirect

Chinese Chemical Letters

journal homepage: www.elsevier.com/locate/cclet

Heterostructures of NiFe LDH hierarchically assembled on MoS_2 nanosheets as high-efficiency electrocatalysts for overall water splitting

Xiao-Peng Li, Li-Rong Zheng, Si-Jie Liu, Ting Ouyang*, Siyu Ye, Zhao-Qing Liu*

School of Chemistry and Chemical Engineering/Institute of Clean Energy and Materials/Guangzhou Key Laboratory for Clean Energy and Materials//Key Laboratory for Water Quality and Conservation of the Pearl River Delta, Ministry of Education, Guangzhou University, Guangzhou 510006, China

ARTICLE INFO

Article history:
Received 1 November 2021
Revised 2 December 2021
Accepted 31 December 2021
Available online 7 January 2022

Keywords:
Transition metal compound
Electrocatalysts
Hydrogen evolution reaction
Oxygen evolution reaction
Overall water splitting

ABSTRACT

Typically, rational interfacial engineering can effectively modify the adsorption energy of active hydrogen molecules to improve water splitting efficiency. NiFe layered double hydroxide (NiFe LDH) composite, an efficient oxygen evolution reaction (OER) catalyst, suffers from slow hydrogen evolution reaction (HER) kinetics, restricting its application for overall water splitting. Herein, we construct the hierarchical MoS_2/NiFe LDH nanosheets with a heterogeneous interface used for HER and OER. Benefiting the hierarchical heterogeneous interface optimized hydrogen Gibbs free energy, tens of exposed active sites, rapid mass- and charge-transfer processes, the MoS_2/NiFe LDH displays a highly efficient synergistic electrocatalytic effect. The MoS_2/NiFe LDH electrode in 1 mol/L KOH exhibits excellent HER activity, only 98 mV overpotential at 10 mA/cm^2. Significantly, when it assembled as anode and cathode for overall water splitting, only 1.61 V cell voltage was required to achieve 10 mA/cm^2 with excellent durability (50 h).

To solve the global energy crisis, developing clean energy technologies is very important [1,2]. Hydrogen, with high weight energy density and zero carbon content, is the focus of research on how to produce hydrogen efficiently. Water splitting consists of two half reactions: hydrogen evolution reaction (HER) and oxygen evolution reaction (OER) [3]. Although current benchmark catalysts for water splitting are noble metal-based (Ir, Ru and Pt) materials, their inherent scarcity severely hinders the large-scale applications [4]. In alkaline conditions, most of non-noble metal OER catalysts with sluggish HER performance, which hamper its application for overall water splitting. Hence, developing non-noble metal bifunctional electrocatalysts is urgent [5–7].

Layered double hydroxides (LDHs) have drawn tremendous research interest for its 2D layered structure with well-defined topology [8–10]. LDH as one of the low-cost materials to replace noble metals OER catalysts [11]. Nevertheless, its poor HER performance is the major drawback that hinders the overall water splitting. Particularly, the Volmer step ($* + H_2O + e^- \rightarrow *H + OH^-$) is rather slow under alkaline conditions and the strong hydrogen coupling ability of LDH [12–14]. Accordingly, many efforts have been made to improve LDH's sluggish HER process. For example, modulates its metal sites surface electronic structure by doping to optimize the Gibbs adsorption energies of H (ΔG_{H^*}) [15,16]. Introducing other metals or defective sites to LDHs can optimize the ΔG_{H^*} to enhance the water splitting performance [14,17-22].

MoS_2 as an efficient HER catalyst with abundant edges, well-aligned and dispersed structure [23,24]. However, due to the improper adsorption energy of OH, its overall water splitting efficiency turned weak. Currently, construction the heterostructure interface to optimize the energy barrier of MoS_2 at the edge location thus improving its water separation performance was confirmed [25,26]. Moreover, structuring heterostructure interfaces allows inheriting properties of individual components along with synergistic effects exceeding single component performance [27]. Also, the HER performance of LDHs materials still demands enhancement due to its inherent poor activity [28]. Feng *et al.* reported a bifunctional electrocatalyst with improved performance in typical 3D hierarchical heterostructures of NiFe LDH [29]. Therefore, a rational heterogeneous structure interface to optimize the adsorption/desorption energy on active sites is feasible to improve overall water splitting performance [16,30].

Here, to predict the MoS_2 coupling with NiFe LDH to optimize its water splitting performance, density functional theory (DFT) calculations are employed. Then, MoS_2/NiFe LDH is obtained in two steps of hydrothermal and electrodeposition on carbon cloth (CC). As evidenced experimentally, MoS_2/NiFe LDH exhibits high

* Corresponding authors.
E-mail addresses: ouyt@gzhu.edu.cn (T. Ouyang), lzqgzu@gzhu.edu.cn (Z.-Q. Liu).

https://doi.org/10.1016/j.cclet.2021.12.095
1001-8417/

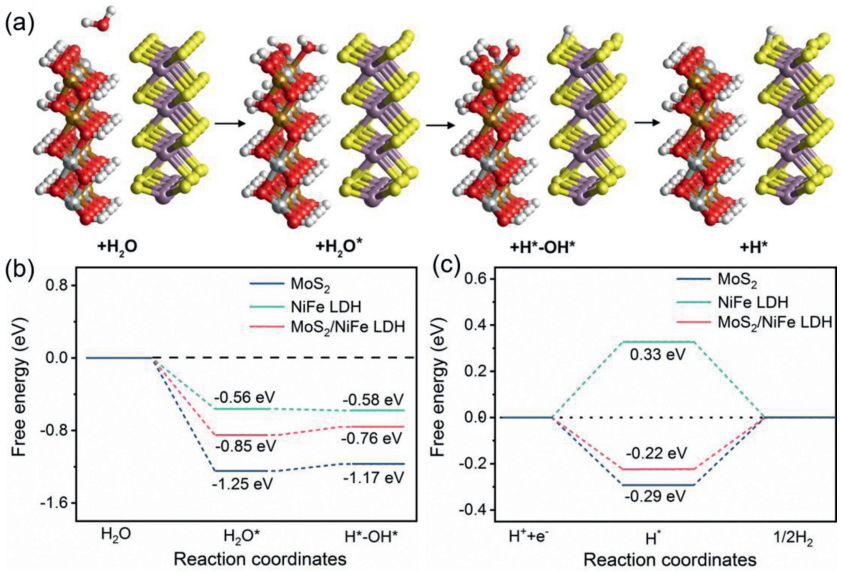

Fig. 1. (a) Schematic representation of HER process of MoS_2/NiFe LDH. The calculated (b) free energy diagram of H_2O adsorption and decomposition process, and (c) HER process of MoS_2, NiFe LDH and MoS_2/NiFe LDH.

HER and OER performance owing to the hierarchical heterogeneous structure and optimized electronic structure. Only 1.61 V cell voltage (to 10 mA/cm^2) is required with robust stability for overall water splitting.

The CC (1 × 3 cm^2) was firstly cleaned to remove surface oil and other contaminants by washing with ethanol, acetone, hydrochloric acid and deionized water in turn under ultrasonic conditions for 10–15 min. Afterwards, Na_2MoO_4 (4 mmol) and CH_4N_2S (8 mmol) were mixed into a uniform 60 mL solution in a Teflon liner with a capacity of 100 mL, the dried CC was immersed in the mixture solution, and heated at 200 °C for 20 h. After the reaction completed, the CC was washed with CH_3CH_2OH and H_2O several times, and then dried at 60 °C.

The synthetic method for MoS_2/CC is based on our previous work. NiFe LDH was prepared by electrodeposition method on the surface of MoS_2/CC. The $Ni(NO_3)_2{\cdot}6H_2O$ (0.15 mol/L) and $FeSO_4{\cdot}6H_2O$ (0.15 mol/L) solution was placed in an H-type electrolyzer and electrodeposited at a constant voltage of −1 V at 35 °C. MoS_2/CC with different NiFe LDH coupling was prepared by controlling the electrodeposition time (160 s, 200 s and 240 s) with Pt sheet as counter electrode, saturated calomel electrode (SCE) as reference electrode. Then, as-prepared samples were washed with H_2O several times, and dried in oven.

Firstly, to comprehend the intrinsic catalytic activity of MoS_2/NiFe LDH, DFT was applied to investigate the ΔG_{H^*}. According to above hypothesis, the theoretical models of MoS_2 and NiFe LDH are constructed to investigate the synergistic optimization of their effect on the Gibbs energy of MoS_2/NiFe LDH. The constructed theoretical models were shown in Fig. 1a and Fig. S1 (Supporting information). In Fig. 1b, the H_2O molecule activation calculation results show the MoS_2 with −1.25 eV energy barrier for rate determining step ($^* + H_2O + e^- \rightarrow {}^*H + OH^-$), higher than that of MoS_2/NiFe LDH (−0.85 eV) and NiFe LDH (−0.56 eV). Moreover, for the H_2O molecule dissociation, MoS_2 with energy barrier of −1.17 eV, higher than that of MoS_2/NiFe LDH (−0.76 eV) and NiFe LDH (−0.58 eV).

Upon analysis of the H_2O adsorption and decomposition processes of the three samples, it can be found the MoS_2/NiFe LDH with heterogeneous interfaces with comparable properties to single MoS_2 and NiFe LDH. Yet, the rate of HER not only depends on the water dissociation, but importantly depends on the ΔG_{H^*} [7,31]. In Fig. 1c, the optimal ΔG_{H^*} of MoS_2/NiFe LDH is −0.22 eV ($^*H + H_2O + e^- \rightarrow {}^* + H_2 + OH^-$). Theoretically, the value of ΔG_{H^*} closer to 0 eV, the more modest H adsorption and desorption intensity of the optimal catalyst is indicated [7]. Verily, comparing the ΔG_{H^*} of single NiFe LDH (0.33 eV) and MoS_2 (−0.29 eV), the MoS_2/NiFe LDH with optimal HER performance. Briefly, the heterogeneous interface of hierarchical coupling of MoS_2 and NiFe LDH can effectively and synergistically promote the HER process by DFT calculation results.

Following, we synthetically prepared the MoS_2/NiFe LDH as predicted. The MoS_2/NiFe LDH is prepared by a two-step method (Fig. 2a). In Fig. 2b, the XRD patterns of the samples are illustrated. The peaks at 14.3°, 29.0°, 32.6°, 35.8°, and 58.3° can attribute to (002), (004), (100), (102), and (110) crystal planes of MoS_2 (PDF #17–0744), respectively. Peaks at 11.5°, 34.5° and 39° are (003), (012) and (015) characteristic crystalline planes belonging to NiFe-LDH (PDF #51–0463). The above XRD patterns confirm the successful synthesis of MoS_2/NiFe LDH. Meanwhile, the performance of NiFe LDH obtained from electrodeposition and hydrothermal methods is verified (Fig. S2 in Supporting information). And its morphology is characterized by scanning electron microscope (SEM, Fig. S3 in Supporting information). Fig. 2c displays the MoS_2 with vertically grown nanosheets uniformly covering the CC with a smooth surface, in contrast to the irregularly stacked nanosheets of the NiFe LDH sheet grown on CC (Fig. S4 in Supporting information). As depicted in Fig. 2d, after rapid electrodeposition, numerous ultrathin NiFe LDH nanosheets grown on the MoS_2 nanosheets surface, forming a layered hierarchical structure. Such a unique structure facilitates the sufficient exposure of active sites on the surface of material. Furthermore, this highly opened structure forms an effective channel for gas emissions during water splitting. The detailed structure is further investigated by transmission electron microscopy (TEM). In Figs. 2e-h, the images show the hierarchical structure of MoS_2/NiFe LDH. Corresponding high-resolution TEM (HRTEM) images of MoS_2/NiFe LDH show lattice spacings of 2.71 Å and 2.30 Å are attributed to the (101) and (015) planes of MoS_2 and NiFe LDH. In Fig. 2i, the corresponding EDS elemental mapping images, the elemental content information is given along with the overall map of the surface spectrum, indicating the Fe,

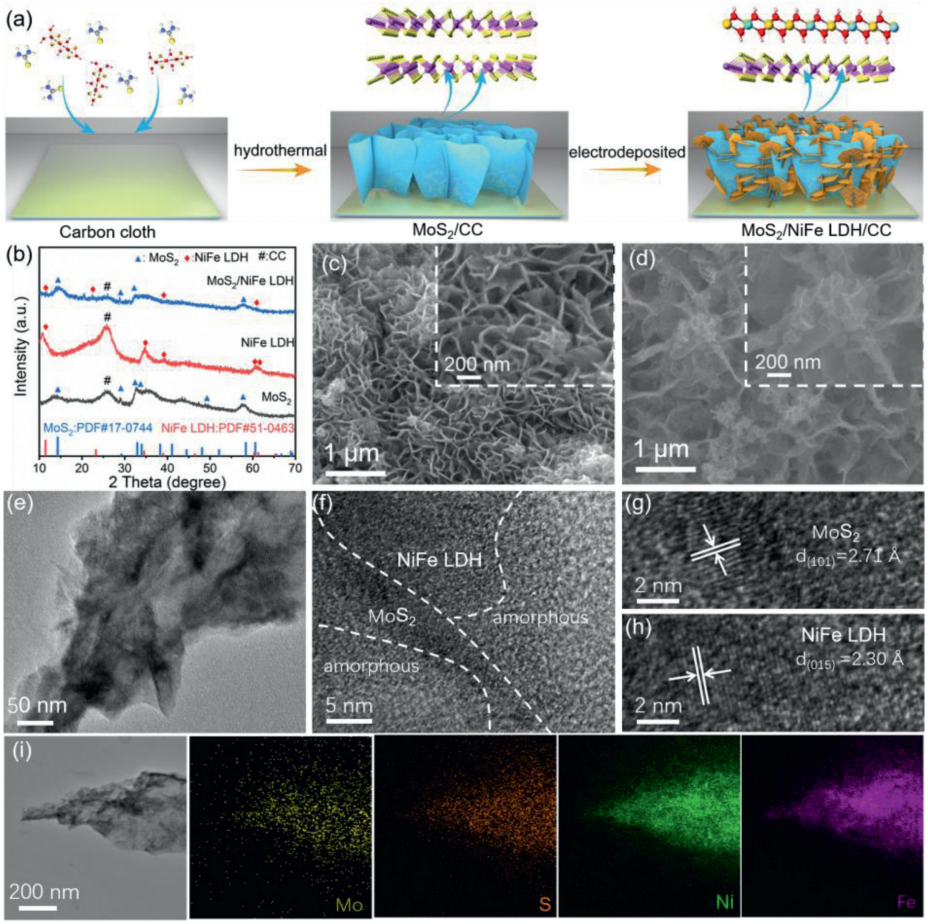

Fig. 2. (a) Schematic illustration of the preparation process for MoS_2/NiFe LDH; (b) XRD patterns of the catalysts, SEM images of (c) MoS_2 NSs, and (d) MoS_2/NiFe LDH; (e) TEM, (f-h) HRTEM images of MoS_2/NiFe LDH, and (i) corresponding EDS images.

Ni, Mo and S are uniformly dispersed the nanosheets (Fig. S5 in Supporting information).

X-ray photoelectron spectroscopy (XPS) was performed to gain a deeper insight on the elemental composition and surface electronic structure of MoS_2/NiFe LDH. The XPS survey spectrum reveals the presence of Mo, S, Ni, and Fe elements in MoS_2/NiFe LDH (Fig. S6 in Supporting information). Ni 2p spectrum shows two spin-orbit peaks Ni $2p_{1/2}$ (872.8 eV) and Ni $2p_{3/2}$ (855.6 eV) in Figs. S7a and b (Supporting information), while the two spin-orbit peaks of the Fe 2p spectrum are located at 711.5 eV/724.8 eV belonging to Fe $2p_{3/2}$/Fe $2p_{1/2}$ [26]. The binding energies of Ni $2p_{3/2}$ and Fe $2p_{3/2}$ in MoS_2/NiFe LDH show a slight negative shift of 0.45 eV and 0.63 eV compared to that of pure NiFe LDH, implying a high electron density (Figs. 3a and b). Fig. S7c (Supporting information) displays the XPS patterns of Mo 3d, the pure MoS_2 exhibits three peaks at 231.87 eV, 228.68 eV and 225.88 eV, corresponding to Mo $3d_{3/2}$, Mo $3d_{5/2}$ and Mo-S. While for the Mo 3d in MoS_2/NiFe LDH, all peaks are slightly shifted to higher energies, indicating that electron transfer has occurred (Fig. 3c) [32]. Based on the fitted data, the appearance of Mo^{6+} for Mo-O may be caused by surface oxidation. Meanwhile, there is a slight positive shift in the S $2p_{3/2}$ binding energies for MoS_2/NiFe LDH with respect to pure MoS_2 (Fig. 3d and Fig. S7d in Supporting information) [24]. Overall, the XPS reveals a strong interface interaction between MoS_2 and NiFe LDH, and it might be beneficial for water splitting process [7,26].

The HER performance of all samples is measured in 1 mol/L KOH solution. Fig. 4a reveals the linear sweep voltammetry (LSV) curves of samples with *iR* compensation. The MoS_2/NiFe LDH shows an obviously smallest overpotential (98 mV to 10 mA/cm^2) than other two. Notably, it only needs overpotential of 178 mV to obtain 50 mA/cm^2 and 221 mV to 100 mA/cm^2 (Fig. S8a in Supporting information). The HER performance of MoS_2/NiFe LDH prepared at various times was examined to investigate the effect of interfacial engineering. The HER activity shows the optimal performance for the electrodeposition of NiFe LDH at 200 s (Fig. S9a in Supporting information). Therefore, a proper NiFe LDH content can improve electrocatalytic performance. In Fig. 4b, the kinetic of catalysts is evaluated by Tafel slope: MoS_2/NiFe LDH (95 mV/dec) < MoS_2 (127 mV/dec) < NiFe LDH (138 mV/dec), suggesting MoS_2/NiFe LDH with the best HER catalytic kinetic activity, also indicates the ability of the heterostructure interfacial coupling of MoS_2 and NiFe LDH to provide efficient mass and charge transfer efficiency for electrocatalytic reactions. The enhanced catalytic performance is associated with its high intrinsic electrical conductivity. Electrochemical impedance spectroscopy (EIS) is conducted to explore the HER kinetics (Figs. S8b and S10 in Supporting information). Obviously, MoS_2/NiFe LDH exhibits a much smaller impedance than MoS_2 and NiFe LDH, in accordance with its better HER performance. Electrochemically active surface (ECSA) with corresponding double layer capacitance (C_{dl}) could be used to estimate its effective number of exposed active sites (Fig. S11 in Supporting information). As expected, the MoS_2/NiFe LDH shows the largest C_{dl}, indicating that more active sites are available in MoS_2/NiFe LDH (Fig. S11d in Supporting information). And the extended ECSA in MoS_2/NiFe LDH should mainly come after NiFe LDH

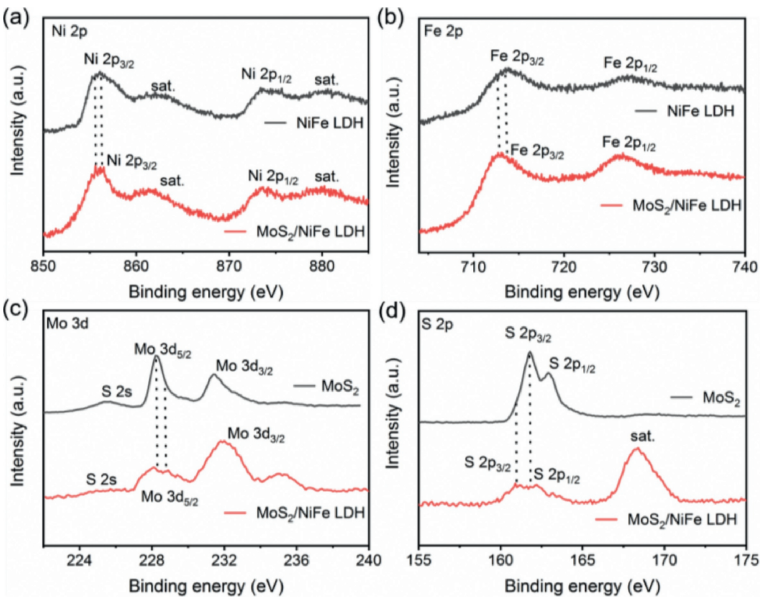

Fig. 3. XPS of the MoS_2/NiFe LDH and the NiFe LDH: (a) Ni 2p, (b) Fe 2p, (c) Mo 3d and (d) S 2p.

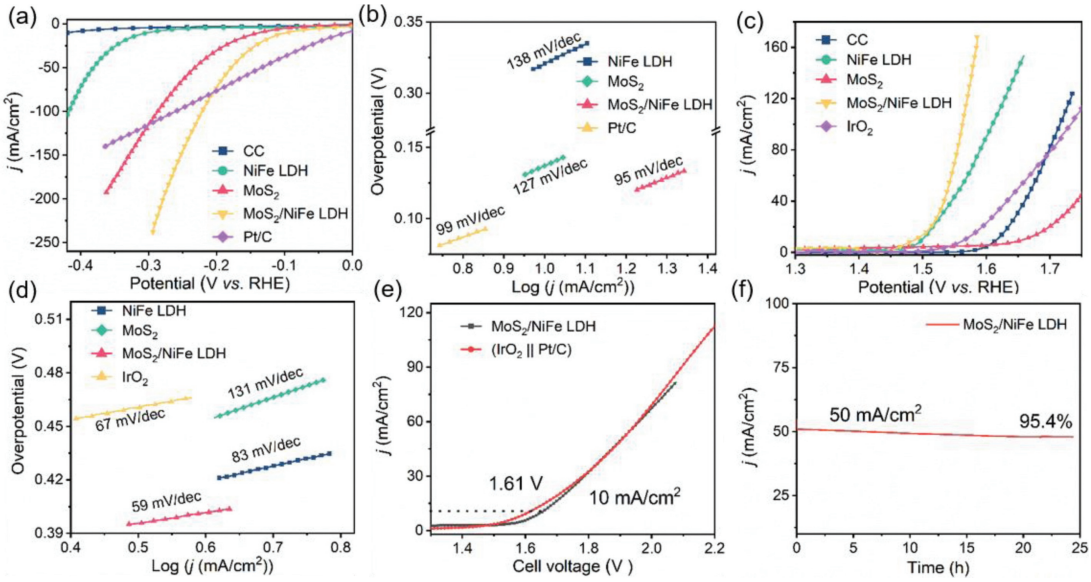

Fig. 4. HER performance: (a) LSV curves, (b) Tafel slopes; OER performance: (c) LSV curves, (d) Tafel slopes; Overall water splitting: (e) LSV curves for MoS_2/NiFe LDH, (f) long-term stability at a current density of 50 mA/cm^2.

electrodeposition. The stability also is important to evaluate the catalyst, the MoS_2/NiFe LDH shows a robust stability as demonstrated through no significant performance loss (97.1%) after 24 h test (Fig. S8c in Supporting information). The crystalline phase after the HER process, suggesting the stability of the catalyst (Fig. S12 in Supporting information). The MoS_2/NiFe LDH with high HER performance could attribute the following reasons: (1) The highly conductive carbon cloth substrate to promote rapid electron transfer and uniform catalyst distribution; (2) the open hierarchy facilitates charge and mass transfer by expanding the contact surface between electrode and electrolyte; (3) the coupled heterostructure creates tens of active sites, and the interference effect modifies the electron structure of catalyst and regulates its ΔG_{H^*}.

The OER performance of the samples is also investigated in 1 mol/L KOH solution. And as expected, MoS_2/NiFe LDH (η_{10} = 257 mV and η_{50} = 308 mV) is superior than NiFe LDH (η_{10} = 268 mV and η_{50} = 327 mV) and MoS_2 (η_{10} = 428 mV and η_{50} = 524 mV) in the as-tested potentials from the *iR*-compensated LSV curves, which reveals that an appropriate NiFe LDH content did significantly boost the OER activity of MoS_2 (Fig. 4c). As shown in Fig. S8d (Supporting information), overpotential of sample at various current densities in OER test are plotted. Similarly, the OER activity of MoS_2/NiFe LDH prepared with different electrodeposition times (160 s, 200 s, 240 s) are tested with findings revealing a trend in line with the HER (Fig. S9b in Supporting information). The Tafel slope of MoS_2/NiFe LDH is 59 mV/dec, lower than the MoS_2 (131 mV/dec) and NiFe LDH (83 mV/dec), indicating its best OER kinetics (Fig. 4d). The OER Nyquist plots show, the impedance of MoS_2/NiFe LDH is obviously lower than the other NiFe LDH and MoS_2, indicating its fastest catalytic kinetics and electron transport (Fig. S8e in Supporting information). And the stability of MoS_2/NiFe LDH is assessed using a long-term chrono-potentiometric method (Fig. S8f in Supporting information). Also, the sample remains in a stable potential range after 24 h of constant testing, implicat-

ing its excellent OER stability. The XRD pattern after the OER reaction reflects that the catalyst can maintain the stability of the crystalline phase after the reaction (Fig. S12 in Supporting information). Through the above results, it demonstrated that the MoS_2/NiFe LDH composite after interfacial coupling had better intrinsic electrocatalytic activity compared with MoS_2 and NiFe LDH.

According to the above results, we employ the MoS_2/NiFe LDH as both cathode and anode for overall water splitting 1 mol/L KOH. Fig. 4e shows the MoS_2/NiFe LDH||MoS_2/NiFe LDH couple drive 10 mA/cm^2 at 1.61 V, which is lower than that of Pt/C||IrO_2 (1.64 V). Meanwhile, Table S1 (in Supporting information) shows the recently reported performance of bifunctional catalysts for overall water splitting. Additionally, the MoS_2/NiFe LDH||MoS_2/NiFe LDH couple also presents remarkable long-term stability and maintained 95.4% of current density after 24 h (Fig. 4f).

In summary, the hierarchical MoS_2/NiFe LDH heterostructure nanosheets are successfully prepared *via* two steps. The elaborate hierarchical layered heterostructure with optimized electronic configuration and chemisorption energy, the large surface area, tens of exposed active sites synergistically enhance the activity of HER and OER. The MoS_2/NiFe LDH for HER can drive 10 mA/cm^2, 50 mA/cm^2, and 100 mA/cm^2 at low overpotentials of 98 mV, 178 mV, and 221 mV, respectively; for OER can drive 257 mV and 308 mV overpotentials to reach 10 mA/cm^2 and 50 mA/cm^2; And the MoS_2/NiFe LDH||MoS_2/NiFe LDH couple drive 10 mA/cm^2 at 1.61 V for overall water splitting.

Declaration of competing interest

The authors declare that they have no known competing financial interests or personal relationships that could have appeared to influence the work reported in this paper.

Acknowledgments

This work was financially supported by National Natural Science Foundation of China (Nos. 21875048 and 21905063), Outstanding Youth Project of Guangdong Natural Science Foundation (No. 2020B1515020028), Guangdong Natural Science Foundation (No. 2021A1515010066), Science and Technology Research Project of Guangzhou (Nos. 201904010052 and 202002010007).

Supplementary materials

Supplementary material associated with this article can be found, in the online version, at doi:10.1016/j.cclet.2021.12.095.

References

[1] P. De Luna, C. Hahn, D. Higgins, et al., Science 364 (2019) eaav3506.
[2] Y. Wang, D. Yan, S. El Hankari, et al., Adv. Sci. 5 (2018) 1800064.
[3] Q. Xu, H. Jiang, X. Duan, et al., Nano Lett. 21 (2021) 492–499.
[4] F. Cheng, L. Wang, H. Wang, et al., Nano Energy 71 (2020) 104621.
[5] J. Cao, C. Lei, J. Yang, et al., J. Mater. Chem. A 6 (2018) 18877–18883.
[6] C. Lei, S. Lyu, J. Si, et al., ChemCatChem 11 (2019) 5855.
[7] X. Luo, P. Ji, P. Wang, et al., Adv. Energy Mater. 10 (2020) 1903891.
[8] K. Huang, R. Dong, C. Wang, et al., ACS Sustainable Chem. Eng. 7 (2019) 15073–15079.
[9] X. Zhang, S. Zhu, L. Xia, et al., Chem. Commun. 54 (2018) 1201–1204.
[10] Y. Hou, M.R. Lohe, J. Zhang, et al., Energy Environ. Sci. 9 (2016) 478–483.
[11] D. Zhou, Y. Jia, X. Duan, et al., Nano Energy 60 (2019) 661–666.
[12] M. Gong, Y. Li, H. Wang, et al., J. Am. Chem. Soc. 135 (2013) 8452–8455.
[13] G.M. Tomboc, J. Kim, Y. Wang, et al., J. Mater. Chem. A: Mater. Energy Sustain. 9 (2021) 4528–4557.
[14] D. Wang, Q. Li, C. Han, et al., Nat. Commun. 10 (2019) 3899.
[15] C. Li, Z. Zhang, R. Liu, Small 16 (2020) 2003777.
[16] Z.W. Gao, J.Y. Liu, X.M. Chen, et al., Adv. Mater. 31 (2019) 1804769.
[17] J. Bao, Z. Wang, J. Xie, et al., Chem. Commun. 55 (2019) 3521–3524.
[18] Q.Q. Chen, C.C. Hou, C.J. Wang, et al., Chem. Commun. 54 (2018) 6400–6403.
[19] G. Chen, T. Wang, J. Zhang, et al., Adv. Mater. 30 (2018) 1706279.
[20] H. Sun, W. Zhang, J.G. Li, et al., Appl. Catal. B 284 (2021) 119740–119752.
[21] P. Li, X. Duan, Y. Kuang, et al., Adv. Energy Mater. 8 (2018) 1703341.
[22] S. Hao, L. Chen, C. Yu, et al., ACS Energy Lett. 4 (2019) 952–959.
[23] C. Zhang, Y. Luo, J. Tan, et al., Nat. Commun. 11 (2020) 3724.
[24] D.C. N.guyena, T.L.L. Doana, S. Prabhakarana, et al., Nano Energy 82 (2021) 105750.
[25] J. Lin, P. Wang, H. Wang, et al., Adv. Sci. 6 (2019) 1900246.
[26] Y. Liu, S. Jiang, S. Li, et al., Appl. Catal. B 247 (2019) 107–114.
[27] Y. Yang, K. Zhang, H. Lin, et al., ACS Catal. 7 (2017) 2357–2366.
[28] B. Zhang, J. Liu, J. Wang, et al., Nano Energy 37 (2017) 74–80.
[29] B. Wang, S. Jiao, Z. Wang, et al., J. Mater. Chem. A 8 (2020) 17202–17211.
[30] L. Wang, Z. Li, K. Wang, et al., Nano Energy 74 (2020) 104850.
[31] J. Hu, C. Zhang, L. Jiang, et al., Joule 1 (2017) 383–393.
[32] J. Zhang, T. Wang, D. Pohl, et al., Angew. Chem. Int. Ed. 55 (2016) 6702–6707.